Article

The Structure–Activity Relationship of CuO in the Catalytic Conversion Reaction of Glycerol to Lactic Acid

Cheng Tang [1], Shuangming Li [1,2,*], Shanqi Li [1], Yiwen Wang [1], Mingyue He [1], Mengyuan Huang [1] and Sansan Yu [1,2,*]

[1] College of Chemical Engineering, Shenyang University of Chemical Technology, Shenyang 110142, China; tc17702438670@163.com (C.T.); 17624219252@163.com (S.L.); 13470061032@163.com (Y.W.); h1953516478@163.com (M.H.); hmy3062@163.com (M.H.)

[2] Key Laboratory of Chemical Separation Technology of Liaoning Province, Shenyang University of Chemical Technology, Shenyang 110142, China

[*] Correspondence: lishuangming@syuct.edu.cn (S.L.); ssyu@syuct.edu.cn (S.Y.); Tel.: +86-24-8938-8453 (S.Y.); Fax: +86-24-8938-3760 (S.Y.)

Abstract: Three types of CuO with different micro–structures were applied to catalyze the conversion of glycerol to lactic acid. The structure–activity relationship between CuO and its catalytic performance was investigated by combining experiments and theoretical calculations. We demonstrated that two CuO samples (CuO–BCC and CuO–CA), as prepared by calcining copper salts, show larger lattice spacing than that of commercial CuO (CuO–COM). In the catalytic experiments, CuO–BCC, which had the largest lattice spacing (d = 0.2480 nm), exhibited the highest yield of 78.54% for lactic acid. The lattice strain caused by lattice expansion was considered more favorable for CuO–BCC in adsorbing glycerol molecules, thereby improving the conversion of glycerol to lactic acid. The DFT simulation calculation results further prove that CuO–BCC has a larger adsorption energy for glycerol and a smaller thermodynamic energy barrier for the dehydrogenation of glycerol to form the key intermediate products (glyceraldehyde and 1,3-dihydroxyacetone) than CuO–COM. This study demonstrates the role of lattice strain effects in the development of catalysts and provides ideas for catalytic glycerol-selective oxidation studies.

Keywords: glycerol; lactic acid; CuO; structure–activity relationship; catalytic oxidation; DFT

1. Introduction

In the context of coping with global climate change, resources and the environment are decisive factors for sustainable economic growth. Efficiency enhancement, emission reduction, and the rational utilization of carbon-based resources are related to the overall state of the country's economy and the people's livelihood [1–3]. In recent years, biodiesel, as a representative renewable liquid fuel, has been gradually increasing in both global production and demand. Glycerol, as the main by-product of the biodiesel production process, is also increasing day by day [4,5]. It is estimated that for every 100 kg of biodiesel produced, 10 kg of glycerol is generated [6,7]. Glycerol has important applications across various fields, including food, medicine, paint, textiles, fuel, and others. The rise and expansion of the biodiesel industry has had a significant impact on the market for glycerol, increasing its production and leading to a sustained decline in its price [8]. However, from another point of view, this also makes glycerol an ideal and low-cost raw material. Undoubtedly, the conversion of glycerol into high-value-added chemical products or raw materials will greatly increase its economic value. This holds considerable potential for development and bears important practical significance [9–11]. Glycerol generates lactic acid, polyglycerol, 1,2-propanediol, glyceric acid, and many other high-value-added derivatives through dehydration, hydrogenolysis, selective oxidation, and other reactions. The efficient utilization of glycerol as a by-product will help to improve the economic

viability of biodiesel industrialization [12,13]. Lactic acid, as one of the products of the selective oxidation of glycerol, has a wide range of applications across various fields, including food, materials, medicine, and daily life [14,15]. The global demand for lactic acid has exceeded its production, underscoring the significant application prospects for the selective oxidation of glycerol to lactic acid [16–21].

Carbohydrates (e.g., glucose and sucrose) can produce lactic acid through biofermentation. However, there are obvious disadvantages, such as low productivity, complex purification methods, and high enzyme costs, in the biofermentation process [22–24]. Compared with traditional fermentation, the catalytic conversion of glycerol to lactic acid has advantages, such as higher productivity and greater cost-effectiveness. So far, the catalysis of glycerol to lactic acid has been divided into two types of reactions: homogeneous and non-homogeneous. Homogeneous reactions are mainly carried out under high-temperature conditions using inorganic bases, such as NaOH and KOH, as catalysts. Kishida et al. [25] first catalyzed the production of lactic acid from glycerol through a hydrothermal reaction in the presence of sodium hydroxide. However, the homogeneous catalytic process requires high-temperature (300 °C) and highly alkaline conditions and is highly corrosive. Non-homogeneous reactions are based on precious or non-precious metal-based catalysts with the addition of inorganic bases. Precious metals mainly include Pt and Au, and are expensive [26,27]. Therefore, studies on the selective oxidation of glycerol to lactic acid have mainly focused on non-precious metals. In the study of non-precious metals, copper-based catalysts have demonstrated their efficacy as good dehydrogenation catalysts, with good economics and efficient catalytic performance [28–30]. Zavrazhnov et al. [31] found that, compared to the homogeneous alkaline catalytic conversion (Ea = 104.0 kJ·mol^{-1}), the synergistic effect of NaOH and copper nanoparticles (Cu NPs) significantly reduced the activation energy of the reaction (Ea = 81.4 kJ·mol^{-1}). Roy et al. [32] found that Cu_2O, functioning as a catalyst, achieved an 80% yield in the conversion of glycerol to lactic acid at 473 K. This reaction was carried out using Cu_2O as the catalyst for the conversion of glycerol to lactic acid. Moreira et al. [33] investigated the generation of lactic acid from copper catalysts (20 wt.% CuO) loaded with carriers of different alkalinities (Al_2O_3, ZnO, and MgO) in a continuous flow reaction apparatus. When the molar ratio of NaOH/glycerol was 1.0, the alkalinity of the carriers had a limited effect on catalytic activity. The selectivity of the different loaded catalysts prepared for lactic acid remained within the range of 80–90%. When the molar ratio of NaOH/glycerol was 0.5, the selectivity of lactic acid increased as the alkalinity of the carriers increased. However, this effect will disappear as the concentration of NaOH increases. Yin et al. [34] found that Cu/MgO and Cu/HAP (hydroxyapatite) catalysts with high alkalinity showed higher catalytic activity in the catalytic conversion of glycerol to lactic acid compared to Cu/ZrO_2 catalysts with low alkalinity. Most of the current studies focus on performance testing of the catalytic reaction. However, there remains a need for further in-depth investigation into the relationship between the structure of the catalyst and catalytic reaction activity, as well as the mechanism of the reaction.

Therefore, combining different catalyst characterization methods and first-principle calculations, this paper explores the structure–activity relationship of three CuO pairs catalyzing the selective oxidation of glycerol to lactic acid. Different characterization methods were used to analyze the morphology and crystalline phase structure of the three CuO samples. The adsorption properties of glycerol on CuO(111) surfaces with different lattice spacings were simulated using density functional theory (DFT). The activation of glycerol molecules on CuO(111) surfaces with different lattice spacings was analyzed using differential charge density studies. Furthermore, the activation of glycerol molecules on CuO(111) surfaces with different lattice spacings was compared according to the Gibbs free-energy curves. The energy barrier of the reaction process on the crystal surface of CuO(111) is influenced by lattice spacing.

2. Results and Discussion

2.1. Characterization

2.1.1. XRD

Figure 1 shows the XRD patterns of the three CuO samples. All the diffraction peaks of the three samples are in good agreement with the JCPDS standard data file 89–5896, belonging to the monoclinic structure of CuO in the C2/c space group (Figure 1a). No other impurity material phase diffraction peaks were found in the XRD spectra, which proved the high purity of the three CuOs. The positions of CuO–COM characteristic diffraction peaks were at 35.57° and 38.77°, respectively, for the (–111) crystallographic plane and the (111) crystallographic plane. In addition, both CuO–BCC and CuO–CA undergo a low-angle shift of the diffraction peaks (2θ angle is undershifted to 38.71°; 38.68°, respectively) compared to CuO–COM (2θ = 38.77°). According to Bragg's law, the diffraction peak is shifted to a smaller angle, indicating that the cell parameters and the lattice spacing become larger.
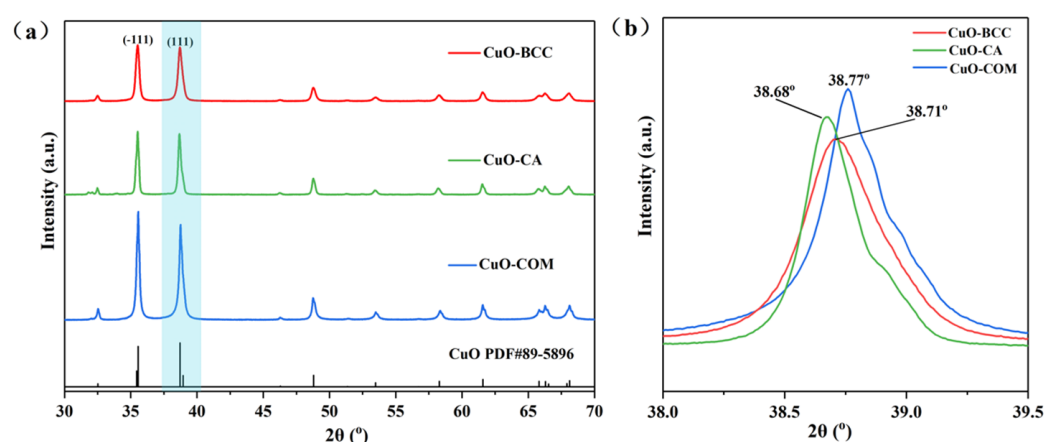
Figure 1. (**a**) XRD spectra of three CuO samples; (**b**) the detailed patterns of the zone marked in blue in (**a**).

2.1.2. SEM and TEM

The SEM, TEM, and HRTEM images of three CuO samples are shown in Figure 2. SEM observed an irregular granular structure for CuO–COM (Figure 2a), a granular stacked structure for CuO–CA (Figure 2d), and a much finer granular structure for CuO–BCC (Figure 2g). TEM observed that CuO–COM had the worst dispersion with severe particle agglomeration (Figure 2b), CuO–CA was poorly dispersed with some particle agglomerated states (Figure 2e), and CuO–BCC was well dispersed (Figure 2h). HRTEM observed that the lattice stripes of CuO–BCC, CuO–CA, and CuO–COM were well defined, and the lattice spacing of CuO–BCC and CuO–CA increased compared to that of CuO–COM (lattice spacing of 0.2338 nm for CuO–COM (Figure 2c), 0.2374 nm for CuO–CA (Figure 2f), and CuO–BCC with a lattice spacing of 0.2480 nm (Figure 2i). HRTEM calculations revealed that CuO–BCC has 6.1% lattice spacing tensile strain compared to CuO–COM, and CuO–CA has 1.5% lattice spacing tensile strain compared to CuO–COM, which proves that lattice expansion exists to different degrees in both CuO–BCC and CuO–CA. This lattice strain caused by lattice expansion may be responsible for the low angle shift of diffraction peaks in XRD for CuO–BCC and CuO–CA.
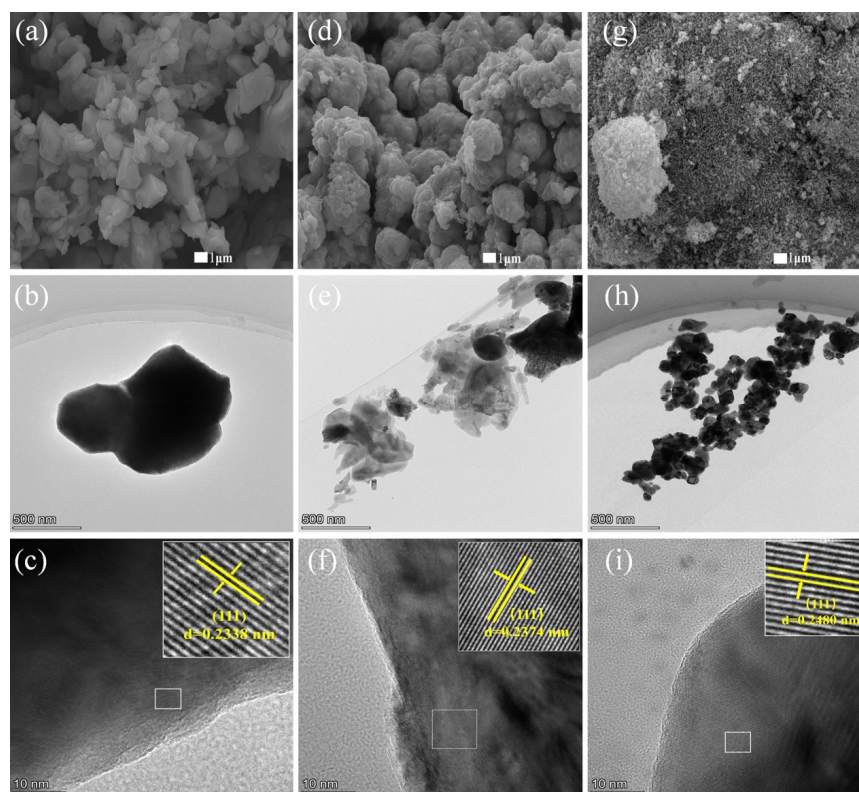
Figure 2. SEM, TEM, and HRTEM images of three CuO samples (**a**–**c**) CuO–COM; (**d**–**f**) CuO–CA; (**g**–**i**) CuO–BCC.

2.1.3. N_2 Adsorption Surface Analysis

The N_2 adsorption/desorption isotherms of the three CuO samples are shown in Figure 3. As can be seen from the figure, all the different sources of CuO have type III isotherms with concave adsorption isotherms, no obvious saturated adsorption plateau, and no inflection point. A clear H3-type hysteresis loop was observed in the range of $0.8 < P/P_0 < 1.0$, and the shape of the hysteresis loops of the three CuOs differed from the relative pressure range. In addition, the specific surface areas of both CuO–BCC and CuO–CA are larger than those of CuO–COM, and the pore radii are smaller than those of CuO–COM. Since the CuO grains themselves do not have a pore structure, the pore structures of the three CuOs measured by the N_2 adsorption method are pore channels formed by the irregular accumulation of CuO grains. The large specific surface area of CuO–BCC and CuO–CA may be attributed to the large dispersion of the CuO grains of CuO–BCC and CuO–CA, which leads to the increase of their specific surface area. CuO–BCC has the largest specific surface area (8.167 m^2/g), and from the adsorption point of view, the larger the specific surface is, the more favorable it is for the adsorption of the reactants on the surface of their catalysts, and the larger the adsorption energy is.

2.1.4. H_2-TPR

H_2-TPR characterization revealed (Figure 4) that the reduction peaks of CuO–BCC and CuO–CA preceded those of CuO–COM, and the peaks were strong and broad, which proved that CuO–BCC and CuO–CA were better dispersed and had stronger oxidizing activity. Combined with the above characterization, the reason may be analyzed as follows: (i) Based on BET observations, CuO–BCC and CuO–CA were found to have a large specific surface area and high dispersion, which increased the reducibility of CuO. (ii) XRD analysis revealed that there was a low angular shift of the diffraction peaks for both CuO–BCC and CuO–CA, and HRTEM calculations revealed that the lattice spacing of CuO–BCC was found to have a higher tensile strain of 6.1% compared to the lattice spacing of CuO–COM,

and the CuO–CA lattice spacing has a 1.5% higher tensile strain than that of CuO–COM. Compared to CuO–COM, CuO–BCC, and CuO–CA, the –Cu–O bond length grows, and –O is more easily stripped. This crystallographic effect exhibited by lattice expansion may be the main reason for the activity enhancement.
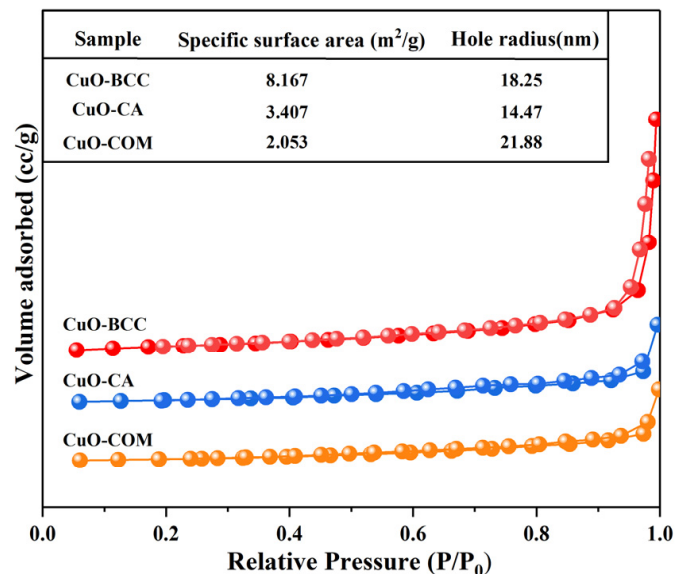
Sample	Specific surface area (m^2/g)	Hole radius(nm)
CuO-BCC	8.167	18.25
CuO-CA	3.407	14.47
CuO-COM	2.053	21.88

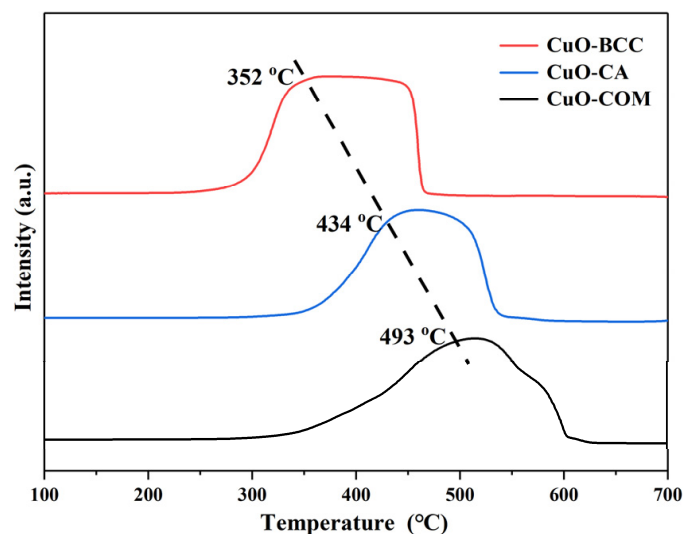**Figure 3.** N_2 adsorption/desorption isotherms of the three CuO samples.

Figure 4. H_2-TPR profiles of the three CuO samples.

2.2. Optimization of Catalytic Reaction Parameters

For the conversion of glycerol to lactic acid, CuO–COM was applied as a catalyst to optimize the catalytic reaction parameters. First, we explored the effect of different types of bases (KOH, NaOH, and Ca(OH)$_2$) on the catalytic activity. The reaction was catalyzed for 6 h at 170 °C with a strong base/glycerol molar amount of 1.1 and a CuO–COM dosage of 2 g (Figure 5a). It was found that different types of bases had different effects on the catalytic glycerol activity, with Ca(OH)$_2$ being less active in catalyzing the conversion of glycerol to lactic acid (46.48% yield for lactic acid). NaOH had the best catalytic activity in catalyzing the conversion of glycerol to lactic acid (72.24% yield for lactic acid). KOH was slightly weaker than NaOH (68.95% yield for lactic acid). The reason for the high catalytic activity of NaOH may be due to its inherent strong alkalinity, which has an outstanding ability to eliminate H from glycerol C_2, thus contributing to the dehydration reaction of

glycerol and its conversion to lactic acid. In the experiments, no intermediate products (i.e., acetone aldehyde, 1,3-dihydroxyacetone, etc.) were found, suggesting that the transition from glycerol to lactic acid is a transient process [31] (p. 2), where the intermediate products will be converted to lactic acid with the increase of the reaction time, and then to lactic acid.
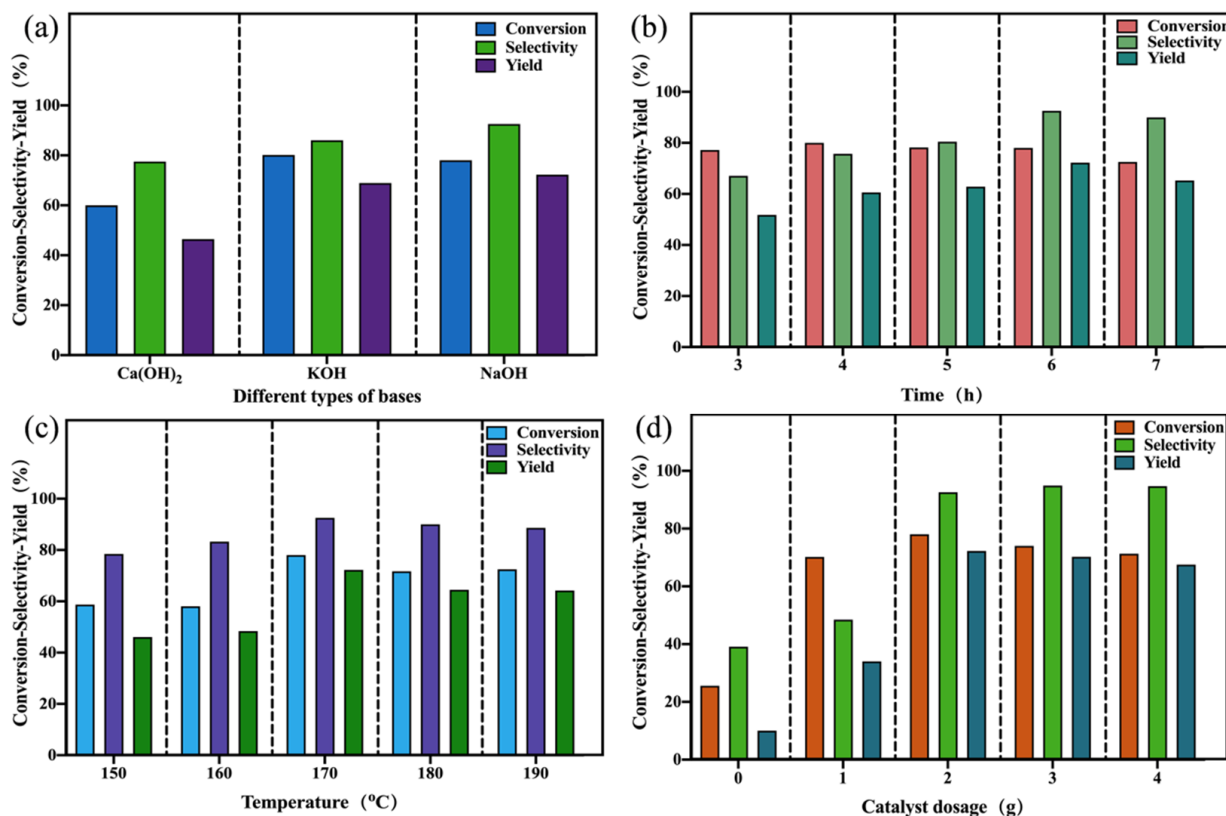
Figure 5. Effect of different factors on catalytic performance (examination of the effect of (**a**) different types of bases; (**b**) reaction times; (**c**) reaction temperatures; and (**d**) catalyst dosages on the catalytic performance using CuO–COM as a catalyst).

Then, we explored the effects of different reaction times on the catalytic activity of catalyzing the conversion of glycerol to lactic acid (Figure 5b). The selective oxidation of glycerol to lactic acid catalyzed by CuO–COM as catalyst (2 g) at 170 °C with a NaOH/glycerol molar ratio of 1.1 showed a more stable trend in the conversion of glycerol with the increase of the reaction time from 3 h to 7 h, whereas the selectivity to lactic acid was increased from 67.09% to 92.56% (Max), and the yield was increased from 51.79% to 72.24% (Max). The increase in reaction time increases the selectivity for lactic acid and hence the yield. However, when the reaction exceeded 6 h, the yield of lactic acid slightly decreased.

Immediately after that, we explored the effect of different reaction temperatures on the catalytic activity of catalyzing the conversion of glycerol to lactic acid (Figure 5c). The selective oxidation of glycerol to lactic acid was catalyzed at different reaction temperatures with CuO–COM as catalyst at a reaction time of 6 h. It was found that the conversion of glycerol increased from 58.73% to 78.05% and then decreased slightly as the reaction temperature was increased from 150 °C to 190 °C, and the selectivity to lactic acid increased from 78.44% to 92.56% and then decreased slightly. The results showed that increasing the reaction temperature was favorable for the catalytic conversion of glycerol to lactic acid.

We explored the effect of catalyst dosage on the catalytic activity under the condition of controlling the reaction time and reaction temperature (Figure 5d). The conversion of glycerol to lactic acid was catalyzed by selecting different catalyst dosages (0, 1, 2, 3, and

4 g) at a reaction temperature of 170 °C, a reaction time of 6 h, and a NaOH/glycerol molar amount of 1.1. It was found that the conversion of glycerol and the selectivity to lactic acid were very low without the addition of CuO (25.59% for glycerol conversion and 39.13% for lactic acid), and that the conversion of glycerol and the selectivity to lactic acid showed a tendency to increase and then stabilize with the addition of CuO–COM. It can be reasonably assumed that the synergistic effect of CuO and NaOH increased the glycerol conversion and selectivity to lactic acid, but was not very effective in catalyzing the selective oxidation of glycerol to lactic acid after CuO–COM exceeded 2 g. The results showed that CuO–COM had no significant effect on the oxidation of glycerol to lactic acid, and the selectivity to lactic acid was 39.13%.

Finally, we explored the effect of NaOH/glycerol molar amounts on the catalytic activity. The reaction was carried out at 170 °C for 6 h with CuO–COM as the catalyst, and NaOH/glycerol molar amounts of 0, 0.5, 1.1, 1.5, and 1.8 were selected. The results are shown in Table 1. It was found that glycerol does not undergo a catalytic reaction in the absence of NaOH addition. Indicating that the addition of NaOH plays an important role in catalyzing the selective oxidation of glycerol, the addition of base may (i) deprotonate glycerol, (ii) promote C–C cleavage of aldehydes or ketones, and (iii) promote the conversion of pyruvic aldehyde to lactic acid. As the molar amount of NaOH/glycerol increased, the conversion of glycerol and selectivity to lactic acid first increased and then stabilized, so adjusting the molar amount of NaOH/glycerol was beneficial to improve the catalytic conversion of glycerol to lactic acid.

Table 1. Effect of different molar amounts of NaOH/glycerol on catalytic performance.

NaOH/Glycerol Molarity	Glycerol Conversion Rate (%)	Lactic Acid Selectivity (%)
0	trace	—
0.5	58.12	81.70
1.1	78.05	92.56
1.5	76.52	93.43
1.8	73.07	93.99

2.3. Structure–Activity Relationship of Three CuO Pairs for Catalytic Reactions

2.3.1. Effect of Three CuO on the Catalytic Performance

Based on the above studies, we chose to investigate the activity of three CuO on catalyzing the selective oxidation of glycerol to lactic acid at 170 °C with a NaOH/glycerol molarity of 1.1 and a reaction time of 6 h (shown in Figure 6). It was found that CuO–BCC and CuO–CA showed better catalytic activity for the selective oxidation of glycerol compared to CuO–COM (72.24% yield of CuO–COM for lactic acid, 78.54% yield of CuO–BCC for lactic acid, and 76.46% yield of CuO–CA for lactic acid). Combined with the above catalyst characterization, the reasons may be: (i) CuO–BCC and CuO–CA have a larger specific surface area and a smaller pore radius than CuO–COM. From the reaction adsorption point of view, the larger the specific surface area and the smaller the pore radius, the more favorable the glycerol adsorption is, thus accelerating the glycerol dehydrogenation step. (ii) HRTEM calculations revealed that CuO–BCC has 6.1% lattice spacing tensile strain compared to CuO–COM, and CuO–CA has 1.5% lattice spacing tensile strain compared to CuO–COM, which proves that there are different degrees of lattice expansion in both CuO–BCC and CuO–CA. Compared to CuO–COM, CuO–BCC and CuO–CA exhibit better dehydrogenation activity due to the increase in –Cu–O bond length and easier stripping of –O. Compared with CuO–CA, CuO–BCC has a larger specific surface area and adsorbs glycerol more easily. Meanwhile, CuO–BCC has a larger lattice spacing tensile strain, its lattice expansion is greater, –O is easier to strip, and the dehydrogenation activity is better.
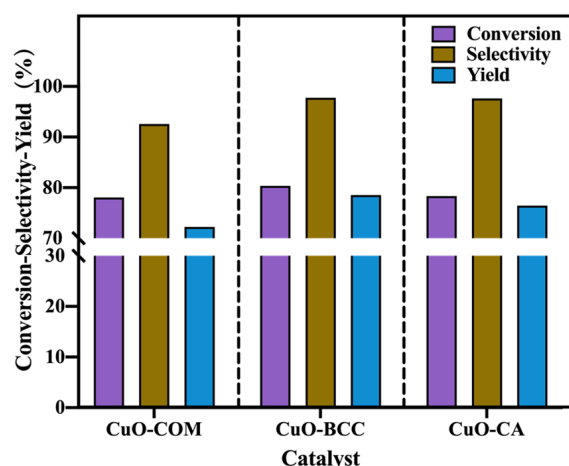
Figure 6. Catalytic performance of the three CuO samples for glycerol-selective oxidation under a reaction temperature of 170 °C, a NaOH/glycerol molarity of 1.1, and a reaction time of 6 h.

2.3.2. Density Functional Theory (DFT) Calculations

In order to compare the difference in activity between CuO–BCC and CuO–CA with CuO–COM in the catalytic conversion of glycerol to lactic acid, density functional theory calculations were used to probe the ontogeny of the activity. Based on the crystal plane information and lattice strain observed in XRD and HRTEM, we built two CuO models: Model I (CuO–COM) and Model II (CuO–BCC). The CuO(111) crystal plane was selected as the crystal plane where the reaction occurred, which is the meritocratic crystal plane we observed in XRD. In addition, based on HRTEM measurements, we set a lattice expansion of 6% in Model II (CuO–BCC). In this way, the effect of the CuO strain on its catalytic performance in converting glycerol to lactic acid was investigated.

Using density functional theory calculations, we modeled the adsorption process of glycerol on two different lattice spacing CuO(111) crystal surfaces (shown in Figure 7). In both models, the hydroxyl oxygen on the primary carbon of glycerol is adsorbed on the Cu site, and the hydroxyl hydrogen on the primary carbon also forms a hydrogen bond with the O on the CuO surface, which facilitates the anchoring and conversion of glycerol in CuO. The adsorption energy calculations show that CuO–BCC containing 6% lattice expansion has a stronger adsorption energy for glycerol (as shown in Table 2). In addition, the simulations revealed that the Cu–O bond lengths formed by glycerol adsorption on the 6% lattice-expanded CuO–BCC are shorter, and the adsorption capacity is stronger relative to the adsorption process of CuO–COM. Further differential charge density analysis (shown in Figure 8) revealed that glycerol adsorbed on the CuO–BCC surface formed a stronger Cu–O charge density, which favored molecular bonding on the surface. On the other hand, the charge transfer from hydrogen to oxygen can be clearly observed due to the hydrogen bonding of the hydroxyl hydrogen on the primary carbon with the oxygen constructed from the CuO surface. The bonding interaction between these two may effectively maintain the stabilization of the structure and protect the dissociation of the hydroxyl hydrogens on the primary carbon, which is further corroborated in subsequent Gibbs free energy calculations. It was also observed that the hydroxyl hydrogen on the sec-carbon of glycerol was more readily activated to produce more 1,3-dihydroxyacetone.

Table 2. Adsorption energy magnitude of glycerol adsorption on CuO(111) crystal surfaces with different lattice spacings versus Cu–O bond length.

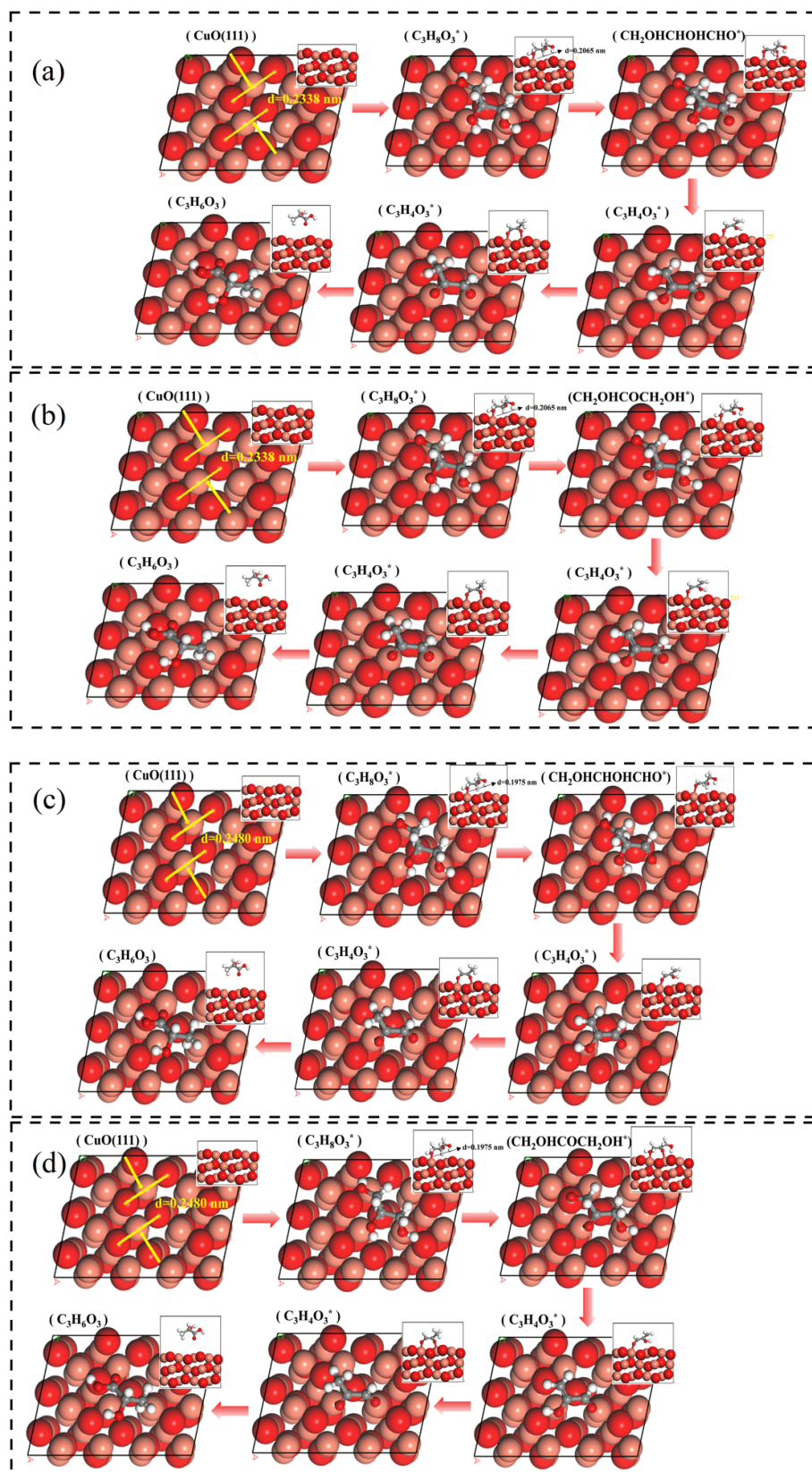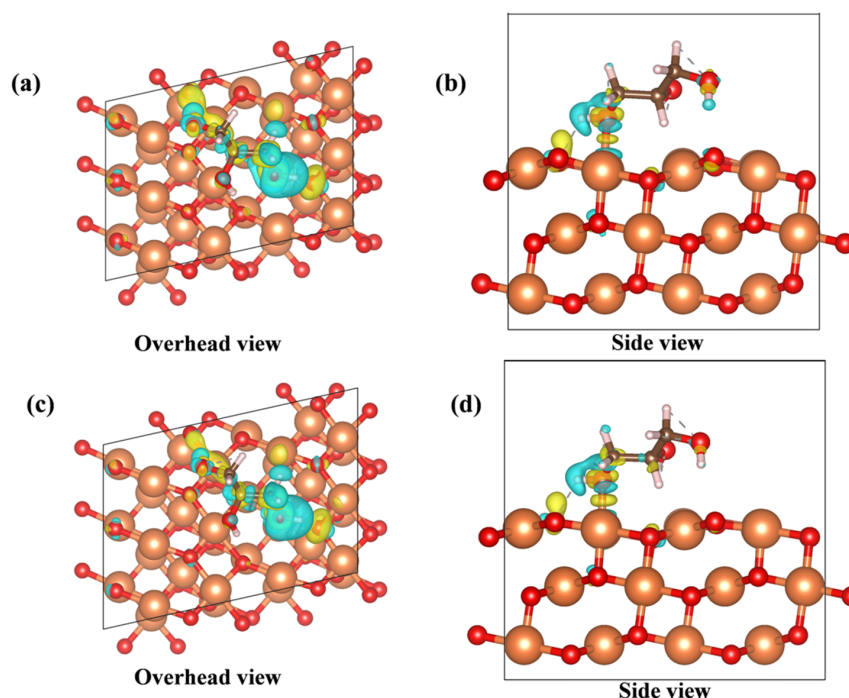| Models	lattice Spacing (nm)	Adsorption Energy (eV)	Cu–O Bond Length (Å)
CuO–COM	0.2338	−3.41	2.0652
CuO–BCC	0.2480	−3.05	1.9753

Figure 7. The adsorption process of glycerol on (111) crystal plane of (**a**,**b**) CuO–COM and (**c**,**d**) CuO–BCC (*: The intermediate is in the adsorbed state).

Figure 8. Differential charge density distribution of glycerol adsorbed on the (111) crystal plane of (**a**,**b**) CuO–COM and (**c**,**d**) CuO–BCC.

The reaction pathway is based on the results reported in previous studies [35–38]. Firstly, glycerol adsorbs on the surface of CuO and thus dehydrogenates to form glyceraldehyde or dihydroxyacetone; the equilibrium between glyceraldehyde and dihydroxyacetone depends on the pH in solution. Subsequently, glyceraldehyde dehydrates to form unstable 2-hydroxyacrolein, which is converted to pyruvic aldehyde via isomerization. Finally, pyruvic aldehyde is rearranged to lactic acid via Cannizzaro (as shown in Figure 9).
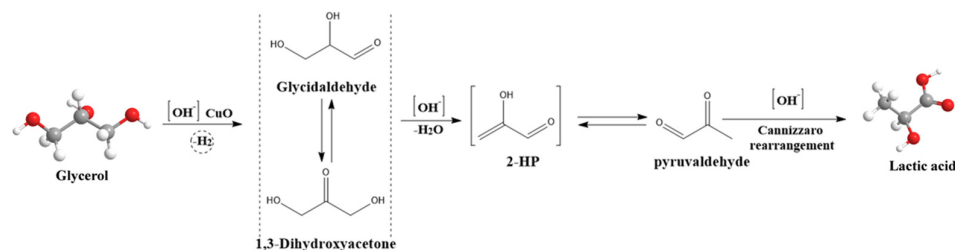
Figure 9. Reaction pathway of glycerol dehydrogenation to lactic acid in an alkaline medium.

Thermodynamic energy analysis of the reaction pathway for the catalytic conversion of glycerol to lactic acid (shown in Figure 10) showed that the rate-limiting step of the reaction is located in the first step of the dehydrogenation of glycerol. Previous mechanisms suggested that dehydrogenation of glycerol might be converted to give either glyceraldehyde or 1,3-dihydroxyacetone, both of which are isomers, so we energetically analyzed both intermediates. Notably, we observed the lowest thermodynamic energy barrier for the dehydrogenation of glycerol to form 1,3-dihydroxyacetone on CuO–BCC (0.43 eV), which is smaller than that for the dehydrogenation of glycerol to form 1,3-dihydroxyacetone on CuO–COM (0.52 eV). Apparently, the strain effect brought about by the lattice expansion is the origin of the activity enhancement of CuO. In addition, it is found that glycerol dehydrogenation to glyceraldehyde is difficult at both CuO–COM and CuO–BCC, because the process has a higher thermodynamic energy barrier (1.03 eV and 1.06 eV) at both CuO–COM and CuO–BCC. This may be due to the fact that the hydroxyl hydrogen on the primary carbon of the glycerol forms a hydrogen bond with the O on the CuO, which effec-

tively maintains the stability of the structure and protects the dissociation of the hydroxyl hydrogen on the primary carbon.
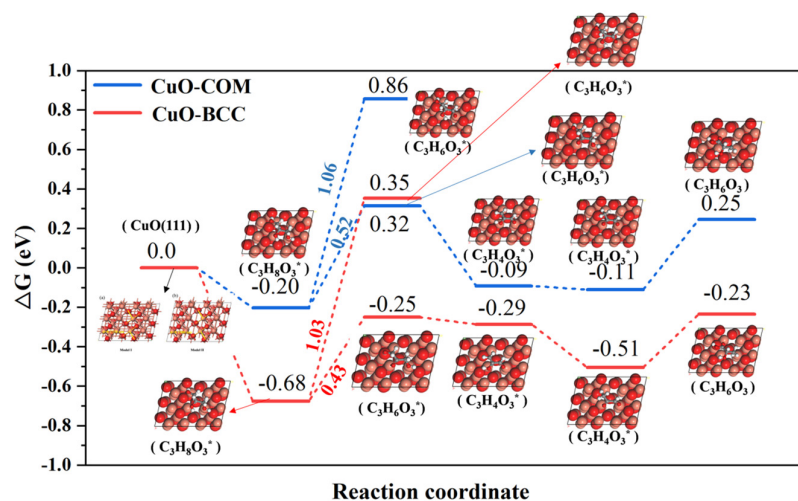
Figure 10. Gibbs free energy diagrams for the catalytic conversion of glycerol to lactic acid on the (111) crystal planes of CuO–COM and CuO–BCC (*: The intermediate is in the adsorbed state).

3. Experimental Section

3.1. Preparation

In this work, three types of copper (II) oxide were used to catalyze the conversion of glycerol, one of which is commercial CuO (hereinafter referred to as CuO–COM) purchased directly, and the other two are obtained through heat treatment of basic copper carbonate ($Cu(OH)_2 \cdot CuCO_3$) and copper acetate (($CH_3COO)_2Cu \cdot H_2O$), respectively.

The typical heat treatment process is as follows: a certain amount of copper salt is calcined at 500 °C for 4 h in an air atmosphere. The as-prepared CuO samples derived from Basic Copper Carbonate and Copper Acetate were referred to as CuO–BCC and CuO–CA, respectively. All the above reagents were analytical reagent (AR) grade and purchased from Sinopharm Chemical Reagent Co, Ltd. (Shanghai, China) and Shanghai Maclin Biochemical Technology Co, Ltd. (Shanghai, China).

3.2. Characterizations

The specific surface area, pore volume, and pore size of the catalyst were determined by an SSA–4300 (Beijing, China) pore size and specific surface area analyzer. The crystalline structure of the catalyst was analyzed by a Smart Lab 9 kW high-resolution X-ray diffractometer (Rigaku RIGAKU, Tokyo, Japan). The test conditions were Cu target Kα rays, a tube voltage of 40 kV, a tube current of 30 mA, a scan rate of 5°/min, and a scan range of 5–80° in steps of 0.02°. The morphology and microstructure of the catalyst were determined by scanning electron microscopy (SEM, JSM–7800F, Tokyo, Japan, test conditions of 20 KV) and transmission electron microscopy (TEM, Talos F200S, Massachusetts, USA, catalyst powder was dispersed in ethanol and sonicated for 30 min, then dropped on a grid of copper mesh for analysis). The reducibility of the catalyst was analyzed by a ChemBET Pulsar type fully automated programmed temperature rise chemisorption instrument (Quantachrome Conta, Florida, FL, USA). The catalyst dosage was 0.1 g. The catalyst was ramped up to 500 °C for 30 min at a rate of 20 °C/min under He atmosphere, and then reduced to 30 °C. He was switched to a mixture of H_2:Ar = 1:9 and ramped to 900 °C at a rate of 10 °C/min.

3.3. Catalytic Tests

The selective oxidation of glycerol to lactic acid was catalyzed by adding a certain amount of CuO as catalyst and 40 wt.% (12 g of glycerol dissolved in 30 g of water) of an aqueous glycerol solution and a certain proportion of NaOH to the microreactor under

air atmosphere at a set reaction temperature and time. After the reaction, the catalyst was removed by centrifugation, and the reaction solution was neutralized to pH 6–7 with 0.6 M H_2SO_4. Quantitative calculations were carried out on an Agilent 1260 liquid chromatograph (Agilent, Santa Clara, CA, USA) equipped with a 250 mm C18 column and a refractive index (RI) detector, and the internal standard was isopropyl alcohol.

The conversion rate of glycerol (X_{GL}), selectivity to lactic acid (S_{LA}), and yield of lactic acid (Y_{LA}) were calculated by Equations (1)–(3), respectively.

$$X_{GL} = (n_{feed}\text{-}n_{remained})/n_{feed} \times 100\% \tag{1}$$

$$S_{LA} = n_{LA}/(n_{feed}\text{-}n_{remained}) \times 100\% \tag{2}$$

$$Y_{LA} = n_{LA}/n_{feed} \times 100\% \tag{3}$$

where n_{feed} and $n_{remained}$ are the initial and remaining molar quantity of glycerol, respectively, in the catalytic reaction system. n_{LA} is the molar quantity of generated lactic acid.

3.4. Model Building and Calculation

All the calculations are performed in the framework of the density functional theory with the projector-augmented plane-wave method, as implemented in the Vienna ab initio simulation package [39]. The generalized gradient approximation proposed by Perdew, Burke, and Ernzerhof is selected for the exchange-correlation potential [40]. The Grimme D3 correction uses a coordination number-dependent dispersion correction [41]. To simulate the catalytic surface to reduce intermolecular interactions, 2×2 Cu (111) supercells were constructed. To avoid interactions between repeated slabs along the z-direction. A vacuum spacing of 15 Å was set in the z-direction between any two repeated slabs to avoid interaction between any two adjacent slabs. The bottom two layers of all slabs were frozen, while the remaining layers were allowed to relax. The cut-off energy for plane waves is set to 450 eV. The energy criterion is set to 10^{-5} eV in the iterative solution of the Kohn–Sham equation. A vacuum layer of 15 Å is added perpendicular to the sheet to avoid artificial interaction between periodic images. The Brillouin zone integration is performed using a $2 \times 2 \times 1$ k-mesh [42]. All the structures are relaxed until the residual forces on the atoms have declined to less than 0.03 eV/Å. Based on the results of crystal plane and lattice spacing obtained by XRD and HRTEM, two models (Figure 11) of the CuO (111) crystal plane with different lattice spacings (d) were constructed to simulate the adsorption process of glycerol on the surface of CuO.
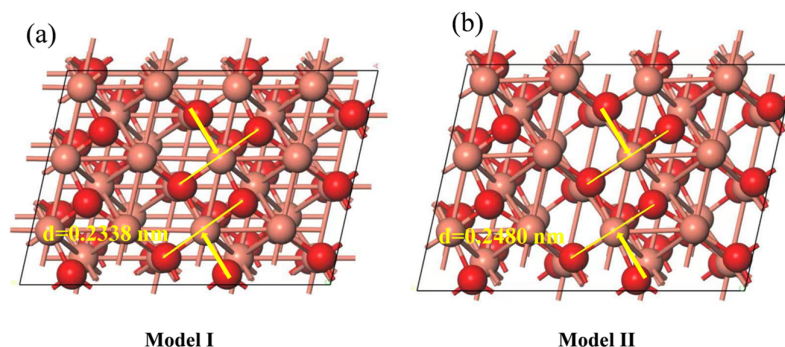
Figure 11. Theoretical models of CuO(111) crystals with different lattice spacings: (**a**) Model I (CuO–COM); (**b**) Model II (CuO–BCC).

The free energy changes (ΔG) of the reaction intermediates were calculated as follows:

$$\Delta G = \Delta E + \Delta E_{ZPE} - T\Delta S \tag{4}$$

where ΔE is the adsorption energy on the cluster surface. ΔE_{ZPE} and ΔS are the differences for zero-point energy and entropy, respectively. The zero-point energy and entropy were

calculated at the standard conditions corresponding to a pressure of 101,325 Pa of H_2 at a temperature of 298.15 K.

4. Conclusions

The structure–activity relationship of three types of CuO in the catalytic conversion of glycerol to lactic acid was investigated. CuO derived from $Cu(OH)_2 \cdot CuCO_3$ and $(CH_3COO)_2Cu \cdot H_2O$ by calcining exhibited a larger lattice spacing than that of commercial CuO, which mainly contributed to the higher glycerol conversion and selectivity to lactic acid. It is concluded that the larger lattice spacing enables CuO to possess greater adsorption energy for glycerol and a smaller thermodynamic energy barrier for glycerol dehydrogenation. Under optimized reaction conditions, the yield of lactic acid from glycerol is as high as 78.54% over CuO–BCC as a catalyst. This lattice strain induced by lattice expansion may be more conducive to the adsorption of glycerol, thus facilitating the selective oxidation of glycerol to lactic acid.

Adsorption energy calculations showed that CuO–BCC had a stronger adsorption energy for glycerol. Further differential charge density analysis found that a stronger Cu–O charge density was formed between glycerol and CuO–BCC, which promoted the activation of glycerol molecules. Meanwhile, the results of the Gibbs free energy diagram of the reaction process indicated that the rate-limiting step of the reaction was located in the first step of the dehydrogenation process of glycerol. Moreover, we observed the thermodynamic energy barrier for the dehydrogenation of glycerol to form 1,3-dihydroxyacetone on CuO–BCC (0.43 eV), which is smaller than that on CuO–COM (0.52 eV).

Author Contributions: Conceptualization, S.L. (Shuangming Li) and S.Y.; methodology, C.T., Y.W. and S.L. (Shuangming Li); formal analysis, C.T. and S.L. (Shuangming Li); data curation, C.T., M.H. (Mingyue He), M.H. (Mengyuan Huang) and S.L. (Shanqi Li); writing—original draft preparation, C.T.; supervision, S.Y. and S.L. (Shuangming Li). All authors have read and agreed to the published version of the manuscript.

Data Availability Statement: Not applicable.

Conflicts of Interest: The authors declare no conflict of interest.

References

1. Chen, S.; Xu, S.; Ge, C.; Hu, C. Mechanistic Investigations of the Synthesis of Lactic Acid from Glycerol Catalyzed by an Iridium–NHC Complex. *Processes* **2022**, *10*, 626. [CrossRef]
2. Wang, F.; Harindintwali, J.D.; Yuan, Z.; Wang, M.; Wang, F.; Li, S.; Yin, Z.; Huang, L.; Fu, Y.; Li, L.; et al. Technologies and perspectives for achieving carbon neutrality. *Innovation* **2021**, *2*, 100180. [CrossRef] [PubMed]
3. Wang, Y.; Guo, C.; Chen, X.; Jia, L.; Guo, X.; Chen, R.; Zhang, M.; Chen, Z.; Wang, H. Carbon peak and carbon neutrality in China: Goals, implementation path and prospects. *China Geol.* **2021**, *4*, 720–746. [CrossRef]
4. Silitonga, A.S.; Atabani, A.E.; Mahlia, T.M.I.; Masjuki, H.H.; Badruddin, I.A.; Mekhilef, S. A review on prospect of Jatropha curcas for biodiesel in Indonesia. *Renew. Sust. Energ. Rev.* **2011**, *15*, 3733–3756. [CrossRef]
5. Oh, P.P.; Lau, H.L.N.; Chen, J.; Chong, M.F.; Choo, Y.M. A review on conventional technologies and emerging process intensification (PI) methods for biodiesel production. *Renew. Sust. Energ. Rev.* **2012**, *16*, 5131–5145. [CrossRef]
6. Willke, T.; Vorlop, K. Biotransformation of glycerol into 1,3-propanediol. *Eur. J. Lipid. Sci. Tech.* **2008**, *110*, 831–840. [CrossRef]
7. Yurdakul, M.; Ayas, N.; Bizkarra, K.; Doukkali, M.E.; Cambra, J.F. Preparation of Ni-based catalysts to produce hydrogen from glycerol by steam reforming process. *Int. J. Hydrogen Energ.* **2016**, *41*, 8084–8091. [CrossRef]

8. Callam, C.S.; Singer, S.J.; Lowary, T.L.; Hada, C.M. Computational analysis of the potential energy surfaces of glycerol in the gas and aqueous phases: Effects of level of theory, basis set, and solvation on strongly intramolecularly hydrogen-bonded systems. *J. Am. Chem. Soc.* **2001**, *123*, 11743–11754. [CrossRef]

9. Zhou, C.H.C.; Beltramini, J.N.; Fan, Y.X.; Lu, G.Q. Chemoselective catalytic conversion of glycerol as a biorenewable source to valuable commodity chemicals. *Chem. Soc. Rev.* **2008**, *37*, 527–549. [CrossRef]

10. Viswanadham, B.; Pavankumar, V.; Chary, K.V.R. Vapor phase dehydration of glycerol to acrolein over phosphotungstic acid catalyst supported on niobia. *Catal. Lett.* **2014**, *144*, 744–755. [CrossRef]

11. Sun, D.; Yamada, Y.; Sato, S.; Ueda, W. Glycerol as a potential renewable raw material for acrylic acid production. *Green Chem.* **2017**, *19*, 3186–3213. [CrossRef]

12. Sagou, J.P.S.; Ahualli, S.; Thomas, F.; Duval, J.F.L. Influence of ionic strength and polyelectrolyte concentration on the electrical conductivity of suspensions of soft colloidal polysaccharides. *J. Colloid Interf. Sci.* **2015**, *459*, 212–217. [CrossRef] [PubMed]

13. Tang, C.; Li, S.M.; Yu, S.S. Research Progress of Solid Catalysts for Catalytic Conversion of Glycerol to Lactic Acid. *J. Mol. Catal.* **2022**, *36*, 398–411.

14. Slomkowski, S.; Penczek, S.; Duda, A. Polylactides—An overview. *Polym. Advan. Technol.* **2014**, *25*, 436–447. [CrossRef]

15. Djukić-Vuković, A.; Mladenović, D.; Ivanović, J.; Pejin, J.; Mojović, L. Towards sustainability of lactic acid and poly-lactic acid polymers production. *Renew. Sust. Energ. Rev.* **2019**, *108*, 238–252. [CrossRef]

16. Reddy, G.; Altaf, M.; Naveena, B.J.; Venkateshwar, M.; Kumar, E.V. Amylolytic bacterial lactic acid fermentation—A review. *Biotechnol. Adv.* **2008**, *26*, 22–34. [CrossRef]

17. Martinez, F.A.C.; Balciunas, E.M.; Salgado, J.M.; González, J.M.D.; Converti, A.; Oliveira, R.P.S. Lactic acid properties, applications and production: A review. *Trends Food Sci. Tech.* **2013**, *30*, 70–83. [CrossRef]

18. Kim, S.Y.; Kim, J.N.; Wee, Y.J.; Park, D.H.; Ryu, H.W. Production of bacterial cellulose by Gluconacetobacter sp. RKY5 isolated from persimmon vinegar. *Appl. Biochem. Biotech.* **2006**, *131*, 705–715. [CrossRef] [PubMed]

19. Lasprilla, A.J.R.; Martinez, G.A.R.; Lunelli, B.H.; Jardini, A.L.; Filho, R.M. Poly-lactic acid synthesis for application in biomedical devices—A review. *Biotechnol. Adv.* **2012**, *30*, 321–328. [CrossRef]

20. Nwamba, M.C.; Sun, F.; Mukasekuru, M.R.; Song, G.; Harindintwali, J.D.; Boyi, S.A.; Sun, H. Trends and hassles in the microbial production of lactic acid from lignocellulosic biomass. *Environ. Technol. Inno.* **2021**, *21*, 101337. [CrossRef]

21. Ghaffar, T.; Irshao, M.; Anwar, Z.; Aqil, T.; Zulifqar, Z.; Asma Tariq, A.; Kamran, M.; Nudrat Ehsan, N.; Mehmood, S. Recent trends in lactic acid biotechnology: A brief review on production to purification. *J. Radiat. Res. Appl. Sci.* **2014**, *7*, 222–229. [CrossRef]

22. Mrillo, B.; Zornoza, B.; De la Iglesia, O.; Téllez, C.; Coronas, J. Chemocatalysis of sugars to produce lactic acid derivatives on zeolitic imidazolate frameworks. *J. Catal.* **2016**, *334*, 60–67. [CrossRef]

23. Auneau, F.; Aranil, S.; Besson, M.; Djakovitch, L.; Michel, C.; Delbecq, F.; Sautet, P.; Pinel, C. Heterogeneous Transformation of Glycerol to Lactic Acid. *Top. Catal.* **2012**, *55*, 474–479. [CrossRef]

24. John, R.P.; Anisha, G.S.; Nampoothiri, K.M.; Pandey, A. Direct lactic acid fermentation: Focus on simultaneous saccharification and lactic acid production. *Biotechnol. Adv.* **2009**, *27*, 145–152. [CrossRef]

25. Kishida, H.; Jin, F.; Zhou, Z.; Takehiko, M.; Heiji, E. Conversion of Glycerin into Lactic Acid by Alkaline Hydrothermal Reaction. *Chem. Lett.* **2005**, *34*, 1560–1561. [CrossRef]

26. Sharninghausen, L.S.; Campos, J.; Manas, M.G.; Crabtree, R.H. Efficient selective and atom economic catalytic conversion of glycerol to lactic acid. *Nat. Commun.* **2014**, *5*, 1–9. [CrossRef]

27. Siddiki, S.M.A.H.; Touchy, A.S.; Kon, K.; Toyao, T.; Shimizu, K. Oxidant-free dehydrogenation of glycerol to lactic acid by heterogeneous platinum catalysts. *ChemCatChem* **2017**, *9*, 2816–2821. [CrossRef]

28. Yang, H.; Chen, Y.; Cui, X.; Wang, G.; Cen, Y.; Deng, T.; Yan, W.; Gao, J.; Zhu, S.; Olabye, U.; et al. A Highly Stable Copper-Based Catalyst for Clarifying the Catalytic Roles of Cu^0 and Cu^+ Species in Methanol Dehydrogenation. *Angew. Chem. Int. Ed.* **2018**, *130*, 1854–1858. [CrossRef]

29. Phung, T.K. Copper-based catalysts for ethanol dehydrogenation and dehydrogenative coupling into hydrogen, acetaldehyde and ethyl acetate. *Int. J. Hydrogen Energ.* **2022**, *47*, 42234–42249. [CrossRef]

30. Wang, Z.; Liu, X.; Rooney, D.W.; Hu, P. Elucidating the mechanism and active site of the cyclohexanol dehydrogenation on copper-based catalysts: A density functional theory study. *Surf. Sci.* **2015**, *640*, 181–189. [CrossRef]

31. Zavrazhnov, S.A.; Esipovich, A.L.; Zlobin, S.Y.; Belousov, A.S.; Vorotyntsev, A.V. Mechanism Analysis and Kinetic Modelling of Cu NPs Catalysed Glycerol Conversion into Lactic Acid. *Catalysts* **2019**, *9*, 231. [CrossRef]

32. Roy, D.; Subramaniam, B.; Chaudhari, R.V. Cu-based catalysts show low temperature activity for glycerol conversion to lactic acid. *ACS Catal.* **2011**, *1*, 548–551. [CrossRef]

33. Moreira, A.B.F.; Bruno, A.M.; Souza, M.M.V.M.; Robinson, L.M. Continuous production of lactic acid from glycerol in alkaline medium using supported copper catalysts. *Fuel Process. Technol.* **2016**, *144*, 170–180. [CrossRef]

34. Yin, H.; Zhang, C.; Yin, H.; Gao, D.; Shen, L.; Wang, A. Hydrothermal conversion of glycerol to lactic acid catalyzed by Cu/hydroxyapatite, Cu/MgO, and Cu/ZrO₂ and reaction kinetics. *Chem. Eng. J.* **2016**, *288*, 332–343. [CrossRef]

35. Ftouni, J.; Villandier, N.; Auneau, F.; Besson, M.; Djakovitch, L.; Pinel, C. From glycerol to lactic acid under inert conditions in the presence of platinum-based catalysts: The influence of support. *Catal. Today* **2015**, *257*, 267–273. [CrossRef]

36. Zavrazhnov, S.A.; Esipovich, A.L.; Danov, S.M.; Zlobin, S.Y.; Belousov, A.S. Catalytic Conversion of Glycerol to Lactic Acid: State of the Art and Prospects. *Kinet. Catal.* **2018**, *59*, 459–471. [CrossRef]
37. Yang, G.Y.; Ke, Y.H.; Ren, H.F.; Liu, C.L.; Yang, R.Z.; Dong, W.S. The conversion of glycerol to lactic acid catalyzed by ZrO$_2$-supported CuO catalysts. *Chem. Eng. J.* **2016**, *283*, 759–767. [CrossRef]
38. Razali, N.; Abdullah, A.Z. Production of lactic acid from glycerol via chemical conversion using solid catalyst: A review. *Appl. Catal. A Gen.* **2017**, *543*, 234–246. [CrossRef]
39. Kresse, G.; Joubert, D. From ultrasoft pseudopotentials to the projector augmented-wave method. *Phys. Rev. B* **1999**, *59*, 1758–1777. [CrossRef]
40. Perdew, J.P.; Burke, K.; Ernzerhof, M. Generalized gradient approximation made simple. *Phys. Rev. Lett.* **1996**, *77*, 3865–3868. [CrossRef]
41. Grimme, S.; Antony, J.; Ehrlich, S.; Krieg, H. A consistent and accurate ab initio parametrization of density functional dispersion correction (DFT-D) for the 94 elements H-Pu. *J. Chem. Phys.* **2010**, *132*, 154104. [CrossRef] [PubMed]
42. Monkhorst, H.J.; Pack, J.D. Special points for Brillouin-zone integrations. *Phys. Rev. B* **1976**, *13*, 5188. [CrossRef]